CEAI, Vol.27, No.4, pp. 41-48, 2025 Printed in Romania

Design, Finite Element Analysis, and Controller Implementation for Deformation of Soft Actuators

Subramanian Meenakshi[1], Gunasekaran Prabhakar[2]

[1]Department of ECE, Thiagarajar College of Engineering,Madurai, India.
(email:smeenakshi@student.tce.edu)
[2]Department of ECE,Thiagarajar College of Engineering,Madurai,India.
(email:gpece@tce.edu)

Abstract: Soft pneumatic actuators, made from elastomeric materials, play a vital role in handling sensitive and delicate items without causing damage. In this work, we explore a structured method for designing and controlling such actuators under a range of pressure conditions. Employing Finite Element Analysis (FEA), a 3D soft actuator is modeled and examined to see how it reacts to various pressure inputs. System identification techniques have been employed to identify the system model from simulated data, guaranteeing stability. Proportional Integral Derivative (PID), Fractional order PID (FOPID) and Model Predictive Controllers (MPC), are designed to manage the actuator's movements across pressure signals between 0 and 30 kPa in order to control free-space deformation. In the time-domain analysis and integral error comparison clearly show that FOPID gives better than the others. A prototype of the soft actuator is fabricated using Ecoflex 00-30 material, enabling real-time prediction and control of its grasp deformations through an FOPID-based electro-pneumatic control setup. The findings are validated by detailed experimental results that include specific data points and graphical representations of the actuator's response to revolutionize industries by offering precise and delicate manipulation capabilities

Keywords: Soft actuator, Finite Element Analysis (FEA), Data-driven, Proportional Integral Derivative (PID), Fractional order PID (FOPID), Model Predictive controller (MPC)

1. INTRODUCTION

Soft robotics has game-changing discipline that connects materials engineering, biology, and control systems to develop compliant robotic system using elastomers. This compliance nature helps a safe interaction with humans and very useful in the complex environments. These systems are composed of elastomeric materials and actuated by pneumatic or hydraulic mechanisms. It offers adaptability, lightweight structure and compliance, making them highly suitable for biomedical, assistive, and underwater applications (Sarker and Islam, 2024; Qin et al., 2023).

Recent developments in soft actuator design have brought bioinspired designs such as cephalopod-inspired suckers (Sholl et al., 2019), modular reconfigurable locomotion systems (Zou et al., 2018), and worm-like robots for constrained tubular environments (Zhang et al., 2019). Additional work on root-inspired self-growing actuators (Sadeghi et al., 2017), robotic fingers (Yang et al., 2017), and tunable grippers (Nasab et al., 2017) demonstrate the range of design innovations improving actuation versatility and grip modulation.

Material modeling is also equally important, when simulating large, nonlinear deformations under various pressure. Hyperelastic silicone rubbers such as Ecoflex have made them popular due to their elasticity and durability. Studies by (Heung et al., 2019; Manns et al., 2018) highlight how additive manufacturing and hyperelastic modeling using Yeoh or Mooney-Rivlin formulations can enhance finite element analysis (FEA) for predicting actuator performance. Other findings from (Kelvin et al., 2019) provide more evidence for a robust FEA-based actuator simulation.

Advanced control strategies are needed to control the system model because soft materials have nonlinear dynamics by nature. Many Modern methods use data-driven modeling, Koopman operator theory, or MPC-based adaptation, whereas traditional PID controllers are frequently improved with fractional-order PID (FOPID) for increased robustness of the controller performance (Thuruthel et al., 2018; Bruder et al., 2019; Wang et al., 2022). Previous research has examined fuzzy plus adaptive cruise systems (Prabhakar et al., 2019), proprioceptive control (Felt et al., 2017), and curvature feedback (Luo et al., 2017), showing the change to model-informed adaptive control.

In this study, we propose an integrated framework that encompasses 3D designing of soft actuator, FEA-based deformation modeling, data-driven modeling for simulated data and control implementation using PID, FOPID and MPC controllers. And real-time protype has been fabricated and validated through experimental results. This work aims to contribute to the development of soft pneumatic actuators suitable for next-generation prosthetic and assistive devices.

2. METHODOLOGY

This section comprises of 3D model design and FEA of the designed model.

2.1. 3D Design

The 3D design of this soft actuator slightly differs from traditional gripper fingers and is intended for perfect grasping of objects, similar to human finger. This soft actuator design lies in its unique use of non-uniform adaptability in gripping a variety of objects.

Unlike traditional grippers with uniform chambers, this design mimics the nuanced movements of a human finger-like curvature, offering superior performance in tasks requiring fine motor skills. It now comprises eight chambers with an internal cavity, as depicted in Figure 1(a) and designed using SolidWorks. It is an effective tool for designing the 3D model. The designed model can be imported into the ANSYS software to simulate and understand the behaviour of the developed soft actuator model.

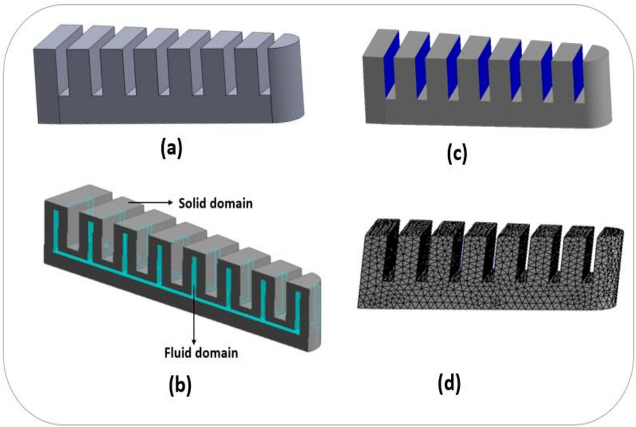

Fig. 1. a. 3D Soft robotic gripper b. Cross sectional view c. Outer wall d. Finite element Meshing.

2.2 Finite Element Analysis (FEA)

Finite element analysis is the mathematical modelling method by solving the partial differential equations to describe the behaviour of the physical model under various loads and boundaries (Kelvin H.L. Heung et al., and Martin Manns et al.,). It discretizes the complex domain into smaller parts called as finite element and these elements are connected as nodes and this formation is known as meshing. In this study, ANSYS is used for Finite Element analysis of the designed model. The first step of this structural analysis is the material selection. Elastomers are the widely used material for soft robots because of its hyper-elastic nature. Various hyper elastic samples are available like Neo-Hookean, Arruda-Boyce, Gent, Mooney-Rivlin, Polynomial, Yeoh and Ogden. Here, Yeoh-2nd order sample has been selected for analysis with the material constants C10=0.7 MPa, C20=0.11 MPa, Incompressibility parameters D1, D2 are set as 0MPa^{-1} which are used to describe the stiffness of the material.

After the selection of material, the designed 3D model is imported into the geometry and then material assignment has been done for solid domain of the model. The outer body of the 8 chambers is considered as a solid domain and the interconnected internal cavity of each chamber is considered as fluid domain (inner wall) as shown in Figure 1(b). The outer side of each chamber i.e., the 14 faces are considered as outer-walls as a shaded part of Figure 1(c). 48 faces of the inner cavity regions of the eight chambers are set as inner-walls.

The mesh utilized in the structural analysis consists of a total of 49,682 nodes and 30,319 elements with the element size of 300 and the meshed model is as shown in Figure 1(d). Now the model is ready for testing. The pressure is applied on the surface of inner-walls and the free space deformation is obtained from the movement of the soft actuator is illustrated as in Figure 2(a). Figure 2(b) illustrates the various free space deformations obtained by changing the input pressure values and the maximum operating pressure range was identified as (0-30) KPa. The maximum deformation of 185.9 mm occurred when applying 28 kPa. Beyond this input pressure value, the solution became unconverged during the simulation.

Equations representing the stress (σ), strain (ε), and deformation (δ) relationship under applied pressure (P) can be represented as (1), (2) and (3):

$$\sigma = E.\varepsilon \tag{1}$$

$$\varepsilon = \frac{\delta}{L_0} \tag{2}$$

$$P = \frac{F}{A} \tag{3}$$

where,

E is the Young's modulus of the material,

L_0 is the original length,

F is the force applied,

A is the cross-sectional area.

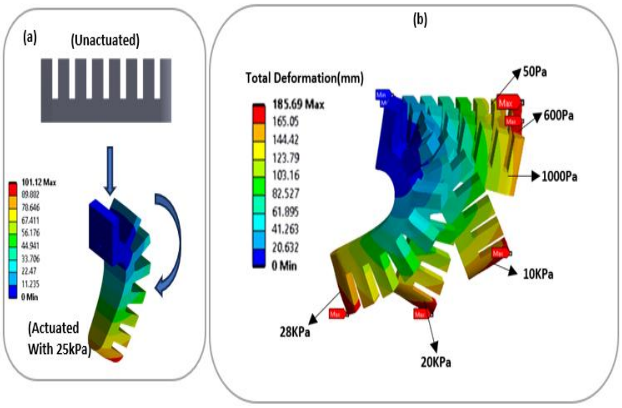

Fig. 2. a. Free space Deformation of Soft actuator for 25Kpa input pressure b. Total deformations for various pressure inputs.

Figure 3(a) and Figure 3(b) illustrates the Equivalent Stress obtained for 10KPa and Equivalent Elastic Strain obtained for 10Kpa. Figure 4 illustrates the relationship between deformation, stress, and strain for a material subjected to 10 KPa pressure. As deformation decreases from 101.12 mm to 11.235 mm, stress significantly drops from 9.323 MPa to 0.149 MPa, and strain decreases proportionally from 0.2725 to 0.0304. This indicates a strong positive correlation between deformation and both stress and strain, with a non-linear relationship between stress and strain. Initially, stress increases rapidly with strain, but the rate of increase diminishes as strain grows. This behaviour is crucial for understanding the material's mechanical properties, especially in applications like soft robotic grippers, where precise control over deformation and stress is essential for handling delicate objects. Soft robots are difficult to model but can be modelled using large-scale data and data-driven modelling methods (Bruder et al., 2019). System identification techniques are employed to derive a transfer function that models the actuator's dynamic response based on FEA results. This transfer function captures the actuator's behaviour in terms of its displacement$u(t)$in response to the input pressure $P(t)$, facilitating the design of control strategies.

$$P(s) = G(s).U(s) \tag{4}$$

where,

$P(s)$ = Laplace transforms of pressure

$U(s)$ = Laplace transforms of displacement

$G(s)$ = Transfer function

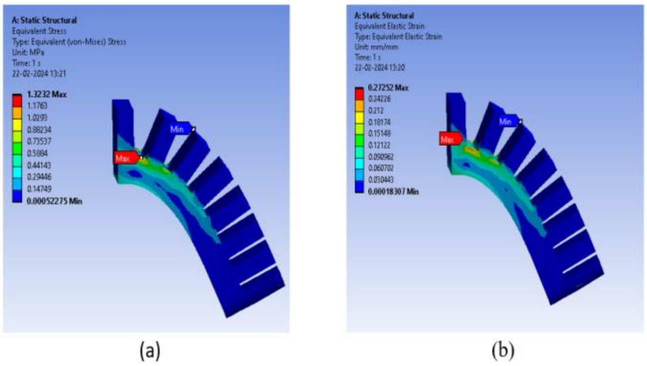

Fig. 3. a. Equivalent Stress obtained for 10KPa input pressure b. Equivalent Elastic Strain obtained for 10KPa input pressure.

3. DATA-DRIVEN BASED SYSTEM IDENTIFICATION

The dataset comprises of input pressure values and their corresponding outputs, representing the total deformation of a soft robotic gripper. These data points were extracted from ANSYS simulations, and their graphical representation is elucidated in Figure 5a, offering a visual insight into the dynamic relationship between the applied pressure and the resulting deformation in the soft actuator. Figure 5a represents collected data samples, where u1 represents the input pressure (KPa), and y1 represents the output deformation of the gripper (mm).

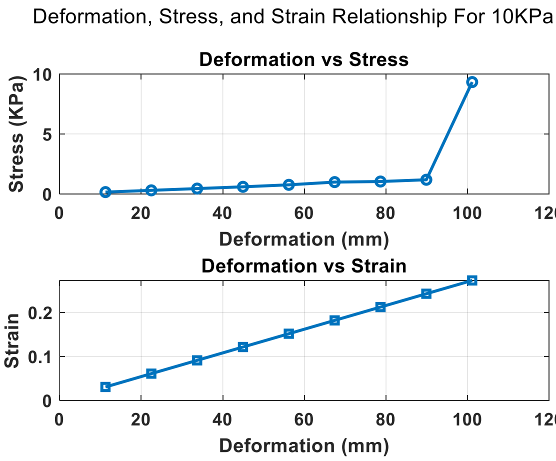

Fig. 4. Relationship between deformation, stress, and strain for 10KPa input pressure.

3.1 Model identification

Linear regression models are used for finding the system from the collected data. 50% of data used for estimation and remaining 50% data used for validation and the various models are used like ARX, ARMAX, BJ, OE. Among them, BJ model gave the highest fit percentage validation results of 93.16% for the values n_a=3, n_b=3, n_c=3, n_d=1, n_f=2, n_k=0 is displayed in Figure 5(b). Figure 5(c) shows that Residual analysis of the Box-Jenkins model that the residuals remain centered around zero with no discernible trend, confirming model stability and unbiased estimation. The low residual amplitude (within ±0.002) and sparse spikes indicate minor random disturbances, affirming the suitability of the BJ model for capturing system dynamics.

The identified System is,

$$G(s) = \frac{5.75e^4 s^2 + 3.667e^4}{s^2 + 0.008232s + 0.0001312} \tag{5}$$

The identified model from the BJ model is considered for further stability analysis and controller design process. Soft robots are notoriously difficult to model, but amenable to large-scale data collection and data-driven modeling methods.

3.2 Stability Analysis

It is important to check the stability of the identified system model. Only then we can determine whether the model is controllable. Here, stability analysis has been conducted using both Pole-Zero plot and Bode plot methods, demonstrating that the identified system is stable.

3.2.1 Pole-Zero plot Analysis

In the figure 6(a) shows that the pole-zero plot displays the system's zeros (shown as blue "o") and poles (shown as red "x") on the complex plane. The places in the s-plane where the system's transfer function goes to infinity are represented by poles, while the places where the transfer function becomes zero are represented by zeros.

By the poles in this plot being in the left-half plane but closer to the right side of the s-plane shows the system is stable. By lowering the response amplitude in particular regions, the zeros, which are situated nearer to the left, assist in stabilizing the system. The transient responsiveness and overall stability of the system are influenced by the relative positions of the poles and zeros.

3.2.2 Bode plot Analysis

Frequency domain components of the system are expressed in the figure 6(b) by the Bode plot: phase (in degrees) and magnitude (in dB) shown over frequency (in rad/s). Magnitude plot shows a low-pass characteristic in which higher frequencies are reduced, with the system's gain decrease as the frequency rises. In Phase Plot, as the frequency rises, the phase progressively increases toward -90° from its initial value near -180°. System with integrative or lagging dynamics typically exhibit this tendency. The magnitude and phase graphs both fulfil the criteria for stability (positive margins), showing that the system is stable.

In the upcoming section, the controller is designed for the system model to control the dynamic behaviour of the designed soft actuator to perform a given task.

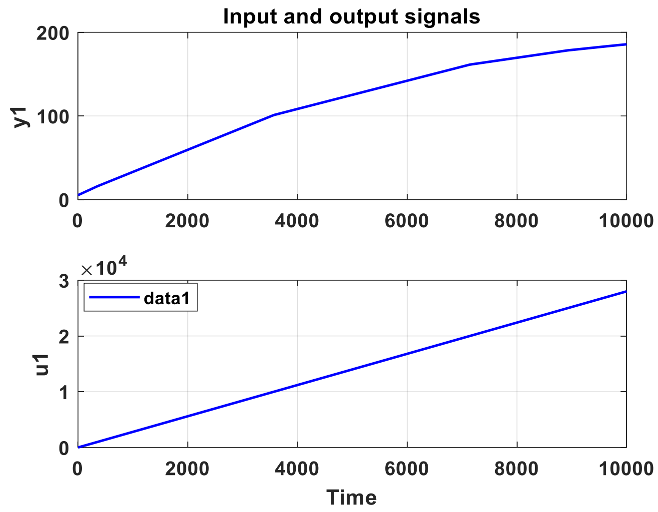

(a)

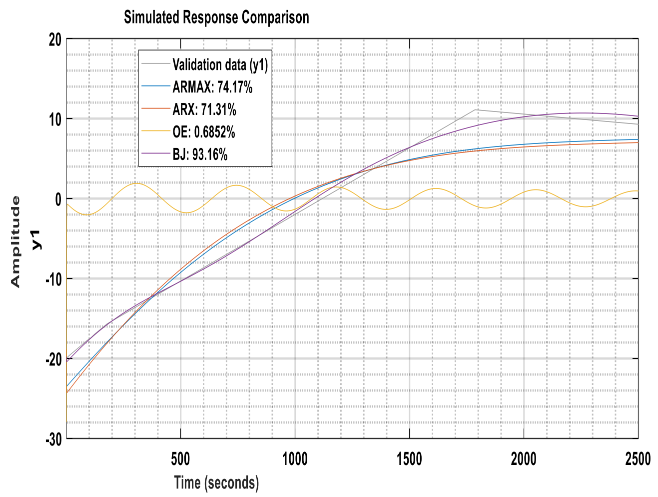

(b)

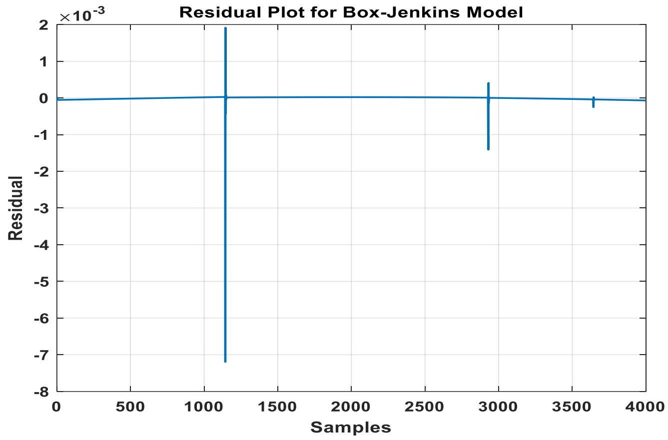

(c)

Fig. 5. a. Collected data samples b. Validation response of various linear regression models c. Residual plot for BJ model.

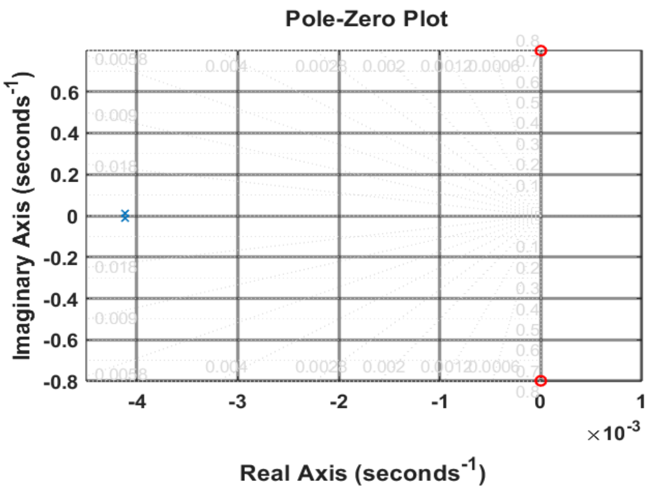

(a)

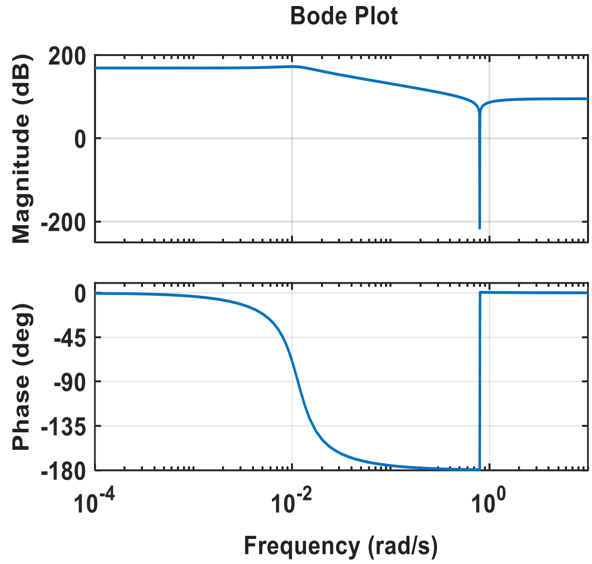

(b)

Fig. 6. Stability Analysis 6. a. Pole-Zero plot 6. b. Bode plot.

4.CONTROLLER DESIGN

4.1 PID Controller

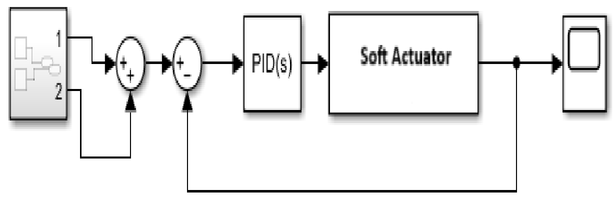

Fig. 7. Structure of PID controller.

The structure of the PID controller as shown in Figure.7. The transfer function of the PID controller is mathematically expressed in (6) (G. Prabhakar et al., 2019).

$$G_c(s) = k_p\left[1 + k_i\frac{1}{s} + k_d\frac{N}{1+N\frac{1}{s}}\right] \tag{6}$$

Where k_p, k_i, k_d&N are proportional gain, integral gain, derivative gain & filter coefficient respectively. Employing an auto-tuning algorithm, the parameters k_p=6.377e-11,

k_i=0.00599, k_d=40.956 and N =16.541 are dynamically selected and integrated into Equation (6). The closed loop performance of PID controller shows that sluggish dynamics and slight overshoot before stabilization, which indicates the need for refinement in the controller structure to achieve faster performance and error reduction for providing the basis of the next step toward FOPID Controller.

4.2 *Fractional-order PID (FOPID) controller*

The general form of FOPID is expressed as (7),

$$U(s) = K_p(1 + \frac{1}{\tau_i s^{\lambda}} + \tau_d s^{\mu}) \qquad (7)$$

where,

$U(s)$- control signal in the Laplace domain.

$E(s)$ - error signal in the Laplace domain.

K_p - proportional gain.

τ_i- integral time constant.

τ_d - derivative time constant.

λ , μ - fractional orders of integration and differentiation, respectively.

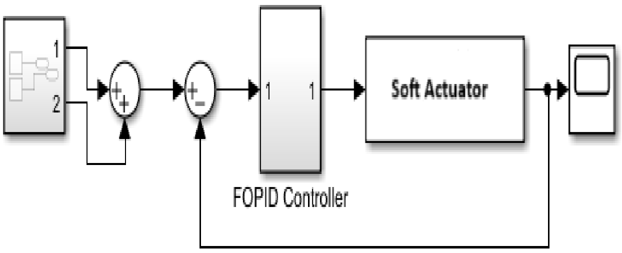

Fig. 8. Structure of FOPID controller.

The equation for the controller in the FOPID controller structure, accounting for fractional orders and parameters, can be expressed as (8):

$$U(s) = K_p\left(\frac{1}{s^{\lambda}}\right)E(s) + K_i\left(\frac{1}{s^{\mu}}\right) + K_{p1}\left(\frac{1}{s^{\vartheta}}\right)E(s) \qquad (8)$$

Where each term corresponds to different fractional operations for the proportional, integral, and derivative actions in the FOPID controller.

FOPID controller as shown in figure 8, which is an improved form of the conventional PID controller. It uses fractional calculus to provide more accurate and flexible control as shown in the block diagram. It utilizes fractional-order operators s^{λ} and s^{μ}, where λ and μ are fractional orders of differentiation and integration, respectively, in contrast to classical PID, which utilizes integer-order differentiation and integration. Using the FOMCON Toolbox, the tuning process aimed to minimize standard time-domain error metrics— ISE (Integral of Squared Error), IAE (Integral of Absolute Error), ITAE (Integral of Time-weighted Absolute Error), and RMSE (Root Mean Square Error)—across a pressure input range of 0–30 kPa. The optimal tuning values obtained were $k_p = 50$, $k_i = 100, and\ k_d = 0.5$, with fractional orders $\lambda = 0.8$ and $\mu = 0.5$. Each term provides improved tuning capabilities to modify to complex system dynamics by working on fractional powers of the Laplace variables.

This is suitable for systems with nonlinearities or memory effects because it enables more precise error correction. The closed loop response of FOPID controller in figure 10 shows that faster response and minimized error. This method gives the system more accurate control by using fractional-order derivatives and integrals. Because of its fractional control, it can better adjust to the dynamics of the system and minimize error more effectively than PID controller. If the system is complex and having constraints, it is difficult to tune to achieve the desired result. For making it the ideal choice for advanced applications requiring predictive and optimized control strategies.

4.3 *Model Predictive Controller (MPC)*

MPC is an advanced control strategy that computes optimal control actions by predicting the future behaviour of a system over a prediction horizon (p) using a system model, while considering constraints on inputs, outputs, and states as shown in the Figure 9. At each time step, it minimizes a cost function, typically of the form (9),

$$J = \sum_{i=1}^{p} \|y(k+i) - r(k+i)\|^2 + \sum_{j=1}^{m} \|\Delta u(k+j)\|^2 \qquad (9)$$

where,

$y(k+i)$ - predicted output,

$r(k+i)$ - reference trajectory and

$\Delta u(k+j)$ - control input change over the control horizon(m).

After solving the optimization problem, only the first control action is applied, and the process repeats at the next time step, making MPC effective for dynamic, multivariable systems under constraints. For this system, controller design for p=10, m=2, Ts=0.001 offering the greatest performance over FOPID controller which is shown in figure 10.

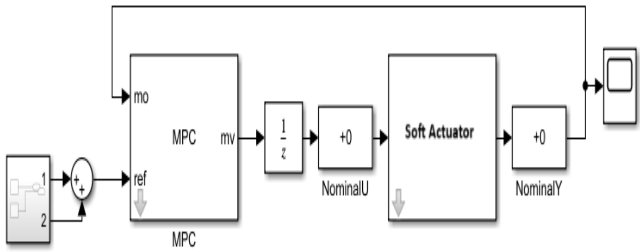

Fig. 9. Structure of MPC controller.

5. CONTROLLER PERFORMANCE ANALYSIS

In the table 1, the error measures like ISE, IAE, ITAE and RMSE are used for evaluating a servo response performance of PID, MPC, and FOPID controllers shown in figure 10. All measures shows that FOPID performs better than the other controllers. PID controller is the least effective of the three due to its largest errors. The most effective control approach overall is FOPID, with MPC coming in second.

Table 2 shows the dynamic performance of three controllers according to overshoot, settling time, and rise time. Although MPC has a large overrun (71.591%), it performs better in rise time (3.232 ms) and settling time (1.2693 ms). In addition, FOPID achieves minimal overshoot (0.505%) and quick rise (3.874 ms) and settling time (2.324 ms).

However, PID performs much worse, with a moderate overshoot (1.994%), a long settling time (1590 s), and a slow rising time (56.82 s). FOPID provides a better trade-off between speed and stability, even though MPC is faster.

Despite having the fastest rise time and a very short settling time, MPC is less than optimal due to its large overshoot, particularly where stability and exact control are crucial.

Table 1. Error Analysis.

	PID	MPC	FOPID
ISE	115.2	0.066320	1.771e-14
IAE	274.0	0.185100	3.678e-08
ITAE	273300.0	0.952400	-2.727e-08
RMSE	0.2113	0.000012	1.689e-08

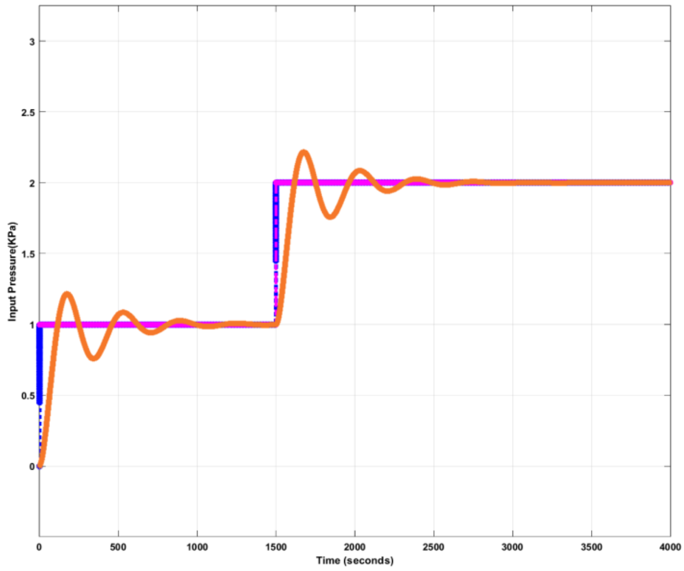

Fig. 10. Closed-loop performance comparison of PID, FOPID, and MPC controllers in tracking input pressure over time. MPC (blue square-dotted line) shows fast rise time with overshoot, FOPID (magenta diamond-solid line) achieves smooth and accurate tracking, and PID (orange star-dashed line) exhibits slower convergence.

Table 2. Time-domain Analysis.

	PID	FOPID	MPC
Rise time(s)	56.82	0.003874	0.003232
Settling time(s)	1590	0.002324	1.269300
Overshoot (%)	1.994	0.505000	71.59100

When settling time and overshoot are taken into account, however, FOPID performs best overall. Because it provides quick stabilization, minimum overshoot, and fast response by comparing to the other controllers.

Therefore, even though MPC is best in some areas, FOPID would still be regarded as the ideal controller for this system because of its superior balance of quick reaction, little overshoot, and quick settling time. For systems where the excessive overshoot can be adjusted or tolerated, MPC might be appropriate; still FOPID is typically the most consistent choice for overall performance. So, the FOPID will be used in real-time implementation of free-space deformation control of the fabricated soft actuator.

6. REAL-TIME IMPLEMENTATION AND CONTROL

6.1. Prototype Fabrication

In this research, a hyper elastic material model was strategically chosen for FEA to effectively simulate the extensive elastic deformations exhibited by the soft actuator under varying pressure inputs. This deliberate selection enabled the characterization of intricate stress-strain relationships critical for accurately predicting the actuator's performance in diverse real-world applications.

Additionally, during the prototype fabrication phase, the SolidWorks-designed actuator was translated into a physical prototype. The real-time soft actuator was fabricated using Ecoflex 00-30 silicone elastomer, which is shown in Figure.11. This material choice was pivotal as it ensured that the fabricated actuator closely matched both the intended geometry and the essential mechanical characteristics required for optimal performance. Ecoflex 00-30, known for its high flexibility, low durometer (00-30 Shore hardness), and excellent tear strength, facilitated the realization of a soft actuator capable of mimicking the behaviours predicted in our FEA simulations.

By including Ecoflex 00-30 in the fabrication process, we ensured that the physical prototype reflects the theoretical predictions closely. This alignment between theoretical simulations and experimental outcomes not only validates our computational models but also supports the reliability and robustness of our research findings. The fabrication process adhered to established methods detailed in references [8-10], ensuring consistency and reliability in the production of the actuator. This integrated approach, from virtual modeling to physical realization using Ecoflex 00-30, underscores the robustness and applicability of our methodology in advancing the capabilities of soft robotics for delicate object manipulation and precision control applications.

6.2. *Experimental Results*

The real-time experimental setup consists of an Arduino Uno interfaced with an electro-pneumatic setup. This arrangement included an air pump, two solenoid valves for air supply and exhaust, and a pressure sensor, flexi-force sensor all under the Model Predictive Control algorithm embedded in the Arduino microcontroller. It allowed for precise regulation of input pressures from 0 to 30 KPa, with the solenoid valves managing air flow for inflating and deflating the soft actuator. Feedback from the pressure sensor and bend sensor are given to the controller and the desired output pressure level is regulated by the FOPID control algorithm. Real-time free space deformations of the fabricated soft actuator for various pressure inputs, as shown in Figure 11 insights impressive deformations and readiness to grasp any objects.

The real-time free space deformation was accurately measured during the actuator's operation and the Figure 12 visualizes how the actuator's tip position changes with increasing pressure. The blue line represents the deformation path, and the red dots indicate the specific tip positions at each pressure level. The experimental deformation values are calculated by Euclidean distance in (10) with the initial position as (0,100),

$$\sqrt{(x2 - x1)^2 + (y2 - y1)^2} \tag{10}$$

Where, $(x1, y1)$ is the initial position of the actuator's tip, $(x2, y2)$ is the subsequent position under increased pressure.

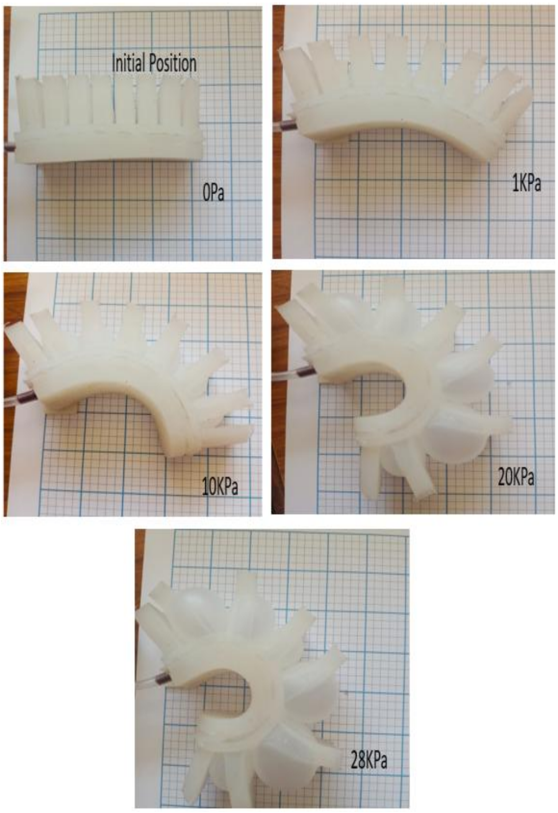

Fig. 11. Real-Time free space deformations of the fabricated soft actuator for various input pressures.

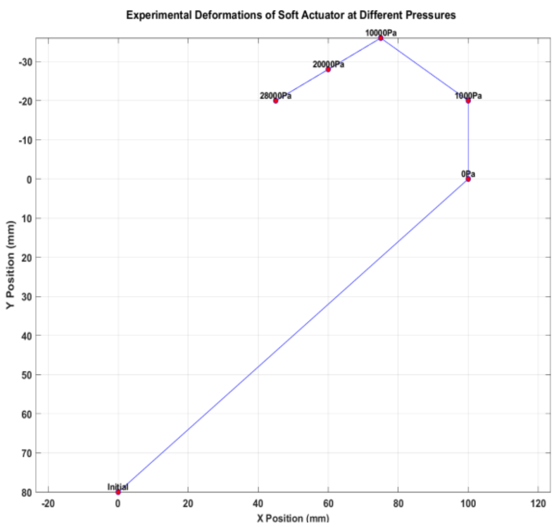

Fig. 12. Actuator's tip position changes with increasing pressure.

Figure 13 compares the free space deformation of the actuator for various pressure signals, both simulated and experimentally obtained. The real-time results indicate deformation levels closely matching those from the simulation.

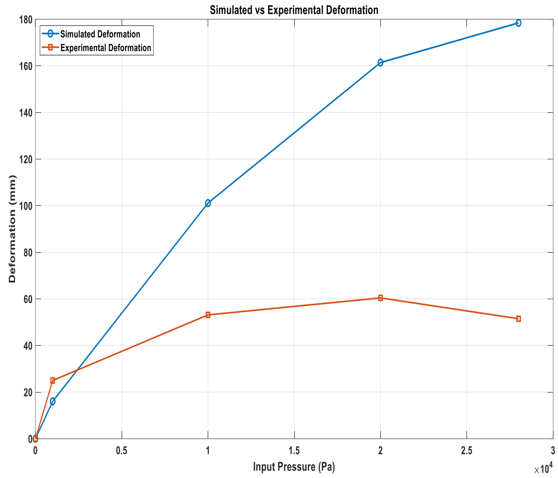

Fig. 13. Comparison of simulated and experimental Deformation results for various input pressure values.

6. CONCLUSION

This research presents an integrated approach to the design, analysis, and control of 3D soft actuator under varying pressure conditions. Using FEA with a hyper elastic material model, we simulated the actuator's free-space deformations and captured key stress-strain relationships. A system model is identified from simulated data ensured stability, forming the basis for implementing both PID, FOPID and MPC. FOPID outperformed the other controllers in terms of time-domain performance and error metrics.

A prototype was fabricated using Ecoflex 00-30, whose flexibility and tear strength closely matched the simulated properties. The real-time control of the actuator's deformations was achieved using an FOPID-based electro-pneumatic setup, demonstrating the potential of soft robotics for precise manipulation tasks. This work validates the computational models and highlights the impact of soft actuators on industries requiring delicate handling and precision.

Future implementations will leverage machine learning-based controllers for soft actuators, significantly enhancing the precision of grasping tasks. By incorporating real-time data and adaptive algorithms, this approach will enable the actuator to respond dynamically to varying object shapes and weights. Additionally, the integration of sensory feedback will allow for more refined control strategies, improving the overall effectiveness and reliability of robotic systems in complex environments. This advancement promises to revolutionize applications in fields such as robotics, prosthetics, and automated manufacturing.

ACKNOWLEDGEMENT

S. Meenakshi thanks Thiagarajar College of Engineering (TCE) for supporting her in this research. Also, the financial support from TCE under the Thiagarajar Research Fellowship scheme (File.no: TRF/Jul-2023/4) is gratefully acknowledged.

REFERENCES

Bruder, D., Remy, C. D., & Vasudevan, R. (2019, May). Nonlinear system identification of soft robot dynamics using koopman operator theory. In *2019 International Conference on Robotics and Automation (ICRA)* (pp. 6244-6250). IEEE.

Chen, B., & Jiang, H. (2019). Swimming performance of a tensegrity robotic fish. *Soft robotics*, *6*(4), 520-531.

Della Santina, C., & Rus, D. (2019). Control oriented modeling of soft robots: The polynomial curvature case. *IEEE Robotics and Automation Letters*, *5*(2), 290-298.

Felt, W., Chin, K. Y., & Remy, C. D. (2017). Smart braid feedback for the closed-loop control of soft robotic systems. *Soft robotics*, *4*(3), 261-273.

George Thuruthel, T., Ansari, Y., Falotico, E., & Laschi, C. (2018). Control strategies for soft robotic manipulators: A survey. *Soft robotics*, *5*(2), 149-163.

George Thuruthel, T., Falotico, E., Manti, M., Pratesi, A., Cianchetti, M., & Laschi, C. (2017). Learning closed loop kinematic controllers for continuum manipulators in unstructured environments. *Soft robotics*, *4*(3), 285-296.

Gul, J. Z., Su, K. Y., & Choi, K. H. (2018). Fully 3D printed multi-material soft bio-inspired whisker sensor for underwater-induced vortex detection. *Soft robotics*, *5*(2), 122-132.

Giannaccini, M. E., Xiang, C., Atyabi, A., Theodoridis, T., Nefti-Meziani, S., & Davis, S. (2018). Novel design of a soft lightweight pneumatic continuum robot arm with decoupled variable stiffness and positioning. *Soft robotics*, *5*(1), 54-70.

Heung, K. H., Tong, R. K., Lau, A. T., & Li, Z. (2019). Robotic glove with soft-elastic composite actuators for assisting activities of daily living. *Soft robotics*, *6*(2), 289-304.

Jusufi, A., Vogt, D. M., Wood, R. J., & Lauder, G. V. (2017). Undulatory swimming performance and body stiffness modulation in a soft robotic fish-inspired physical model. *Soft robotics*, *4*(3), 202-210.

Kastor, N., Vikas, V., Cohen, E., & White, R. D. (2017). A Definition of Soft Materials for Use in the Design of Robots. *Soft robotics*, *4*(3), 181-182.

Khaldi, B., Harrou, F., Benslimane, S. M., & Sun, Y. (2021). A data-driven soft sensor for swarm motion speed prediction using ensemble learning methods. *IEEE Sensors Journal*, *21*(17), 19025-19037.

Luo, M., Skorina, E. H., Tao, W., Chen, F., Ozel, S., Sun, Y., & Onal, C. D. (2017). Toward modular soft robotics: Proprioceptive curvature sensing and sliding-mode control of soft bidirectional bending modules. *Soft robotics*, *4*(2), 117-125.

López-Díaz, A., Vázquez, A. S., & Vázquez, E. (2024). Hydrogels in soft robotics: past, present, and future. *ACS nano*, *18*(32), 20817-20826.

Manns, M., Morales, J., & Frohn, P. (2018). Additive manufacturing of silicon based PneuNets as soft robotic actuators. *Procedia Cirp*, *72*, 328-333.

Meenakshi, S., Prabhakar, G., Ayyanar, N., & Pugazhenthi, P. N. (2023, December). Fem based soft robotic gripper design for seaweed farming. In *2023 International Conference on Energy, Materials and Communication Engineering (ICEMCE)* (pp. 1-5). IEEE.

Nasab, A. M., Sabzehzar, A., Tatari, M., Majidi, C., & Shan, W. (2017). A soft gripper with rigidity tunable elastomer strips as ligaments. *Soft robotics*, *4*(4), 411-420.

Prabhakar, G., Selvaperumal, S., & Nedumal Pugazhenthi, P. (2019). Fuzzy PD plus I control-based adaptive cruise control system in simulation and real-time environment. *IETE Journal of Research*, *65*(1), 69-79.

Qin, L., Peng, H., Huang, X., Liu, M., & Huang, W. (2024). Modeling and simulation of dynamics in soft robotics: A review of numerical approaches. *Current Robotics Reports*, *5*(1), 1-13.

Rodrigue, H., Wang, W., Han, M. W., Kim, T. J., & Ahn, S. H. (2017). An overview of shape memory alloy-coupled actuators and robots. *Soft robotics*, *4*(1), 3-15.

Robertson, M. A., Sadeghi, H., Florez, J. M., & Paik, J. (2017). Soft pneumatic actuator fascicles for high force and reliability. *Soft robotics*, *4*(1), 23-32.

Sholl, N., Moss, A., Kier, W. M., & Mohseni, K. (2019). A soft end effector inspired by cephalopod suckers and augmented by a dielectric elastomer actuator. *Soft robotics*, *6*(3), 356-367.

Sadeghi, A., Mondini, A., & Mazzolai, B. (2017). Toward self-growing soft robots inspired by plant roots and based on additive manufacturing technologies. *Soft robotics*, *4*(3), 211-223.

Sarker, A., Ul Islam, T., & Islam, M. R. (2025). A Review on Recent Trends of Bioinspired Soft Robotics: Actuators, Control Methods, Materials Selection, Sensors, Challenges, and Future Prospects. *Advanced Intelligent Systems*, *7*(3), 2400414.

Sood, S. K., Rawat, K. S., & Sharma, G. (2022). Role of enabling technologies in soft tissue engineering: a systematic literature review. *IEEE Engineering Management Review*, *50*(4), 155-169.

Wang, J., Xu, B., Lai, J., Wang, Y., Hu, C., Li, H., & Song, A. (2022). An improved Koopman-MPC framework for data-driven modeling and control of soft actuators. *IEEE Robotics and Automation Letters*, *8*(2), 616-623.

Xavier, M. S., Tawk, C. D., Yong, Y. K., & Fleming, A. J. (2021). 3D-printed omnidirectional soft pneumatic actuators: Design, modeling and characterization. *Sensors and Actuators A: Physical*, *332*, 113199.

Yang, Y., Chen, Y., Li, Y., Chen, M. Z., & Wei, Y. (2017). Bioinspired robotic fingers based on pneumatic actuator and 3D printing of smart material. *Soft robotics*, *4*(2), 147-162.

Zou, J., Lin, Y., Ji, C., & Yang, H. (2018). A reconfigurable omnidirectional soft robot based on caterpillar locomotion. *Soft robotics*, *5*(2), 164-174.

Zhang, B., Fan, Y., Yang, P., Cao, T., & Liao, H. (2019). Worm-like soft robot for complicated tubular environments. *Soft robotics*, *6*(3), 399-413.

Zimmermann, S. A. (2023). *Data-Driven Modeling of Robotic Manipulators–Efficiency Aspects*. Linkopings Universitet (Sweden).